Local cross-correlation model of stereo correspondence

Martin S. Banks[*a], Sergei Gepshtein[a], & Heather F. Rose[b]
[a]Vision Science Program, University of California, Berkeley, CA USA 94720-2020
[b]Boengineering Program, University of California, Berkeley, CA, USA 94720-1762

ABSTRACT

As the disparity gradient of a stimulus increases, human observers' ability to solve the correspondence problem and thereby estimate the disparities becomes poorer. It finally fails altogether when a critical gradient—the disparity-gradient limit (Burt & Julesz, 1980)—is reached. We investigated the cause of the disparity-gradient limit. As part of this work, we developed a local cross-correlator similar to ones proposed in the computer vision literature and similar to the disparity-energy model of neurons in area V1. Like humans, the cross-correlator exhibits poorer performance as the disparity gradient increases. We also conducted a psychophysical experiment in which observers were presented sawtooth waveforms defined by disparity. They made spatial phase discriminations. We presented different corrugation spatial frequencies and amplitudes, and measured observers' ability to discriminate the two phases. Coherence thresholds (the proportion of signal dots at threshold relative to the total number of dots in the stimulus) were well predicted by the disparity gradient and not by either the spatial frequency or amplitude of the corrugation waveform. Thus, human observers and a local cross-correlator exhibit similar behavior, which suggests that humans use such an algorithm to estimate disparity. As a consequence, disparity estimation is done with local estimates of constant disparity (piecewise frontal), which places a constraint on the highest possible stereo resolution.

I. INTRODUCTION

In estimating disparity, it is essential to match features in the left eye with appropriate features in the right eye. The problem of matching appropriate features is the stereo correspondence problem. The problem is most striking in the random-dot stereogram (Julesz, 1971). The elements in such stimuli, unlike features in the natural environment, do not differ in size, shape, luminance, or color, so information from the elements themselves does not restrict the number of possible pairings of the left and right eyes' images. The problem for the visual system is to distinguish the few correct pairings from the many incorrect ones. The means by which the correspondence problem is solved has been a very active research area. Many computational models have been proposed, but they can be divided more or less into two classes: models in which candidate matches are evaluated with respect to matching constraints and models based on inter-ocular correlation.

Models using explicit matching constraints work as follows (Nelson, 1975; Marr & Poggio, 1976, 1979; Mayhew & Frisby, 1980; Grimson, 1981; Pollard et al., 1985; Prazdny, 1985). The positions of a set of features are measured in both eyes' images. The features may be descriptive elements such as zero-crossings. The possible matches between those features are then evaluated with respect to matching constraints. The similarity constraint mandates that features of similar type are matched (e.g., similar size). The uniqueness constraint requires that for every feature in one eye there is a match to one and only one in the other eye. The smoothness constraint biases the system toward a solution in which the disparities generally do not change markedly between adjacent regions in the image (which is another way of saying that the solution should be consistent with a smooth depth map). By invoking the constraints, these models are generally able to discard false matches in favor of correct ones.

Disparity estimation by computing inter-ocular correlation has also been studied extensively (Tyler & Julesz, 1978; Jenkin & Jepson, 1988; Cormack et al., 1991; Kanade & Okutomi, 1994; Weinshall & Malik, 1995; Cox et al., 1996; Banks et al., 2004). Furthermore, the properties of binocular neurons in striate cortex suggest that disparity estimation begins with signals closely related to binocular correlation measured after the image is filtered by monocular receptive fields (Ferster, 1981; Qian & Zhu, 1997). Indeed, Fleet et al. (1996; Eqns. 20 & 21) and Anzai et al. (1999; Eqns. 5-8) pointed out the mathematical equivalence between inter-ocular correlation and the disparity-energy calculation that underlies binocular interaction in V1 neurons (Ohzawa et al., 1990; Cumming & Parker, 1997; Prince et al., 2002).

In matching by inter-ocular correlation, a patch in one eye's image is correlated with patches of similar size in the other eye's image. Barnard and Fischler (1987) pointed out that the patch size must be large enough to include sufficient intensity variation. If the patch is not large enough, the disparity estimate will be poor because the signal (luminance variation) to noise ratio is low. On the other hand, if the image region of interest contains significant depth variation, the

patch cannot be too large because the inter-ocular correlation will yield an estimate close to the average disparity and fail to detect the disparity variation. Kanade and Okutomi (1994) developed a binocular-matching algorithm that searches for the optimal patch size and shape; it finds the patch size and shape for each image location that yields the disparity estimate of least uncertainty. In image regions with significant depth variation, small patches yield the best disparity estimate; in regions with little depth variation, large patches do the best.

It is interesting to note that the three matching constraints listed earlier—similarity, uniqueness, and smoothness—can all be thought of as byproducts of the computation of inter-ocular correlation. Similarity is favored because high correlations occur when the candidate features are similar in size, shape, contrast polarity, etc. Uniqueness is favored because high correlations occur when the same number of features is presented in the two patches. Smoothness is favored because the correlation between image patches where disparity changes is lower than the correlation between patches where disparity is constant.

II. THE DISPARITY-GRADIENT LIMIT

In the classical literature, the largest fusable disparity is described in terms of Panum's area (Ogle, 1950). Tyler (1973), Braddick (1979), and Burt and Julesz (1980) showed that this description misses something fundamental. They showed that the disparity gradient, not the disparity amplitude, determines the ability to solve the correspondence problem when object points are near one another in the 2D visual field.

The disparity gradient is the rate of change of disparity with change in position in the visual field. A pair of horizontally separated points forms angles α_L and α_R at the left and right eyes. The disparity is $\delta = \alpha_L - \alpha_R$. The angular separation is $x = (\alpha_L + \alpha_R)/2$. The disparity gradient is the ratio: $\delta/x = 2(\alpha_R - \alpha_L)/(\alpha_L + \alpha_R)$. The gradient is zero for points with zero disparity (points on the horopter) and infinite for points aligned in depth (points with zero angular separation). Burt and Julesz showed that whenever the gradient reaches a critical value, stereo correspondence breaks down even when the object points are within Panum's area. The critical value is the disparity-gradient limit and is ~1 for all tilts (i.e., directions of slant).

The disparity-gradient limit has played a prominent role in theories of stereo correspondence. Several models invoke a gradient limit of ~1 in an attempt to cull false matches (e.g., Pollard et al., 1985; Prazdny, 1985). Others use a smoothness constraint that is nearly equivalent (e.g., Marr & Poggio, 1976; Mayhew & Frisby, 1980; Grimson, 1981). In both cases, the justification is that the probability of a match being a false one is much greater when the match implies a large gradient than when it implies a small one. This argument is stronger for opaque than for transparent surfaces. Another related justification is that with opaque surfaces, the disparity gradient will be less than 2 for points visible to both eyes (Trivedi & Lloyd, 1985).

It is important to point out that the disparity-gradient limit can be thought of as a byproduct of solving correspondence by computing correlation. A key feature of matching by correlation is that the correlation is highest when the two eyes' images, once shifted horizontally into registration, are similar. Because of this, the highest correlations are observed when the disparity gradient is 0, which can only occur when the stimulus is tangent to the Vieth-Müller Circle. For simplicity, we will only consider the case in which the surface lies straight ahead, where the Vieth-Müller tangent is a fronto-parallel plane. We speculate that the visual system solves the binocular-matching problem with a procedure like the inter-ocular correlation and, as a consequence, disparity estimates are those associated with piecewise frontal surface patches. In a study of disparity-selective cells in V1, Nienborg et al. (2004) came to the same conclusion.

III. LOCAL CROSS-CORRELATION MODEL

Our model was inspired by the computational work of Kanade and Okutomi (1994). As we said, Kanade and Okutomi showed that adaptive window sizes (that is, the part of the image in one eye that is correlated with an image of like size in the other eye) are required for effective disparity estimation in realistic scenes. Larger windows are required for image regions with gradual luminance variation and smaller windows are required for regions where depth variation is large. To investigate further, we constructed a correlation algorithm for estimating disparity. The inputs to the algorithm were the stimuli used in our experiments convolved with the point-spread function of the well-focused eye.

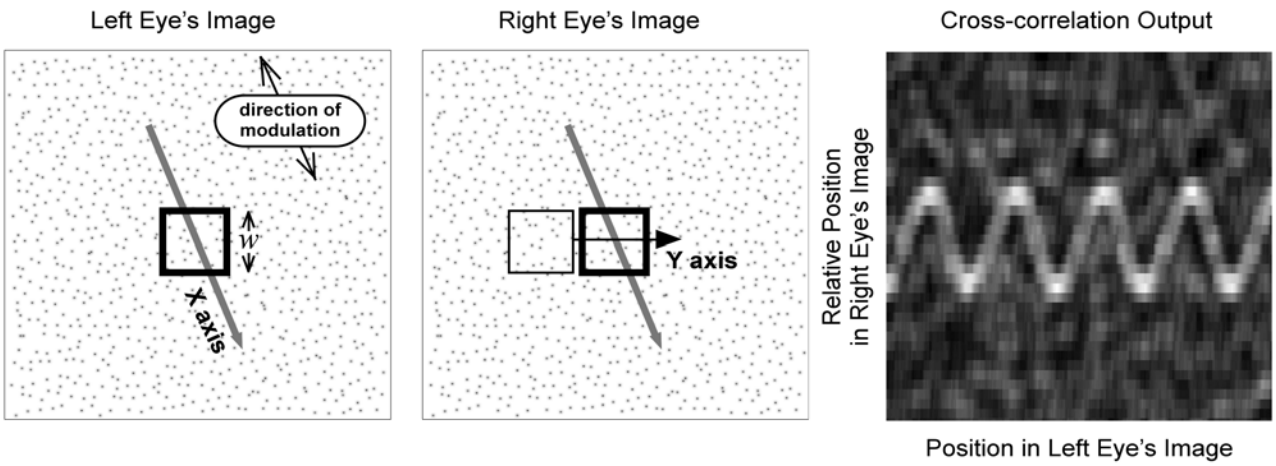

Figure 1. Schematic of the correlation algorithm for binocular matching. The left and middle panels are the images presented to the left and right eye. The corrugation waveform is oriented 20° counter-clockwise from horizontal. A square correlation window (it was actually a circular Gaussian) was placed in the left eye's image (the thick square). That window was moved on a line (oblique arrow) through the middle of the image and in a direction orthogonal to disparity corrugation. For each position of the left eye's window, a square window of the same size was placed in the right eye's image (thin square; again actually a circular Gaussian). We restricted the movement of the right eye's window to a horizontal line (horizontal arrow) through the midpoint of the left eye's window. For each position of the left eye's window, we computed the cross-correlation between the two windowed images. The right panel shows the output. The abscissa is the position of the window in the left eye's image (along the oblique arrow) and the ordinate is the relative position of the window in the right eye's image (along the horizontal arrow), i.e., horizontal disparity. The scale of the ordinate has been magnified relative to the scale of the abscissa. Correlation is represented by intensity, brighter values corresponding to higher correlations.

The main features of the binocular-matching algorithm are depicted in Figure 1. A circular (actually a 2D Gaussian) correlation window W_L was placed in the left eye's image. That window was moved on a line through the middle of the image and orthogonal to disparity corrugation. For each position of the left eye's window, a circular window W_R was placed in the right eye's image. We capitalized on the epipolar constraint and restricted the movement of the right eye's window to a horizontal line (horizontal arrow) through the midpoint of the left eye's window. For each position of the left eye's window, we computed the cross-correlation between the two windowed images:

$$c(\delta_x) = \frac{\sum_{(x,y)\in W_L} [(L(x,y)-\mu_L)(R(x-\delta_x,y)-\mu_R)]}{\sqrt{\sum_{(x,y)\in W_L}(L(x,y)-\mu_L)^2}\sqrt{\sum_{(x,y)\in W_L}(R(x-\delta_x,y)-\mu_R)^2}}$$

The image intensities were $L(x,y)$ and $R(x,y)$ for the left and right eyes, and the mean intensity within each window was μ_L and μ_R. The cross-correlation c was computed for all horizontal shifts δ_x of the right eye's image relative to the left eye's.

An example of the output is displayed on the right in Figure 1. The x-axis is the window's position in the left eye's image and the y-axis is the window's horizontal position in the right eye's image relative to the left eye's (the horizontal disparity δ_x). Correlation is represented by the gray-scale value. There is a ridge of high correlation corresponding to the sinusoidal disparity waveform, so in this case the algorithm detected the signal.

We have examined a number of properties of this model of stereo correspondence and compared those properties to the behavior of human observers. Much of this work is presented in Banks et al. (2004). Here we examine in more detail one important property: the effect of the disparity gradient on the ability to estimate disparity, but first we briefly review other model properties.

Banks et al. (2004) investigated how the best window size for disparity estimation depends on the density of samples in the stimulus and found that window size must be large enough to incorporate on average ~1 dot (meaning that many image regions allow more than 1 dot per window):

$$w = 1/\sqrt{d}$$

where w is the window diameter and d is the dot density (in dots/deg^2). Banks and colleagues also found that the critical number of samples per window depends on the luminance spatial-frequency content of the monocular images. Banks et al. (2004) next examined how the best window size for disparity estimation depends on corrugation frequency. Disparity estimation is excellent when the window is small relative to the period of the corrugation waveform (provided enough dots in the window). Disparity estimation is poor when the window is large relative to the period of the corrugation: the estimate is like a thickened fronto-parallel plane rather than the sinusoidal waveform. The window width must be as small as or smaller than a half cycle of the corrugation waveform:

$$w = \frac{1}{2f}$$

where f is the spatial frequency of the corrugation waveform. Thus, shrinking the correlation window can significantly improve disparity estimation when dot density and corrugation frequency are high.

IV. THE EFFECTS OF DISPARITY GRADIENT ON THE MODEL'S PERFORMANCE

In the correlation framework, solving the matching problem is tantamount to finding similar filter outputs from the two eyes. For the outputs of matched filters to be similar, their inputs must be similar, so binocular matching in this scheme requires similar local intensity patterns in the left and right eye's images. The local patterns in the two eyes are quite different when the disparity gradient is high because a large gradient in part of the binocular stimulus means that one image is stretched (tilt = 0) or sheared horizontally (tilt = 90 deg) relative to the other.

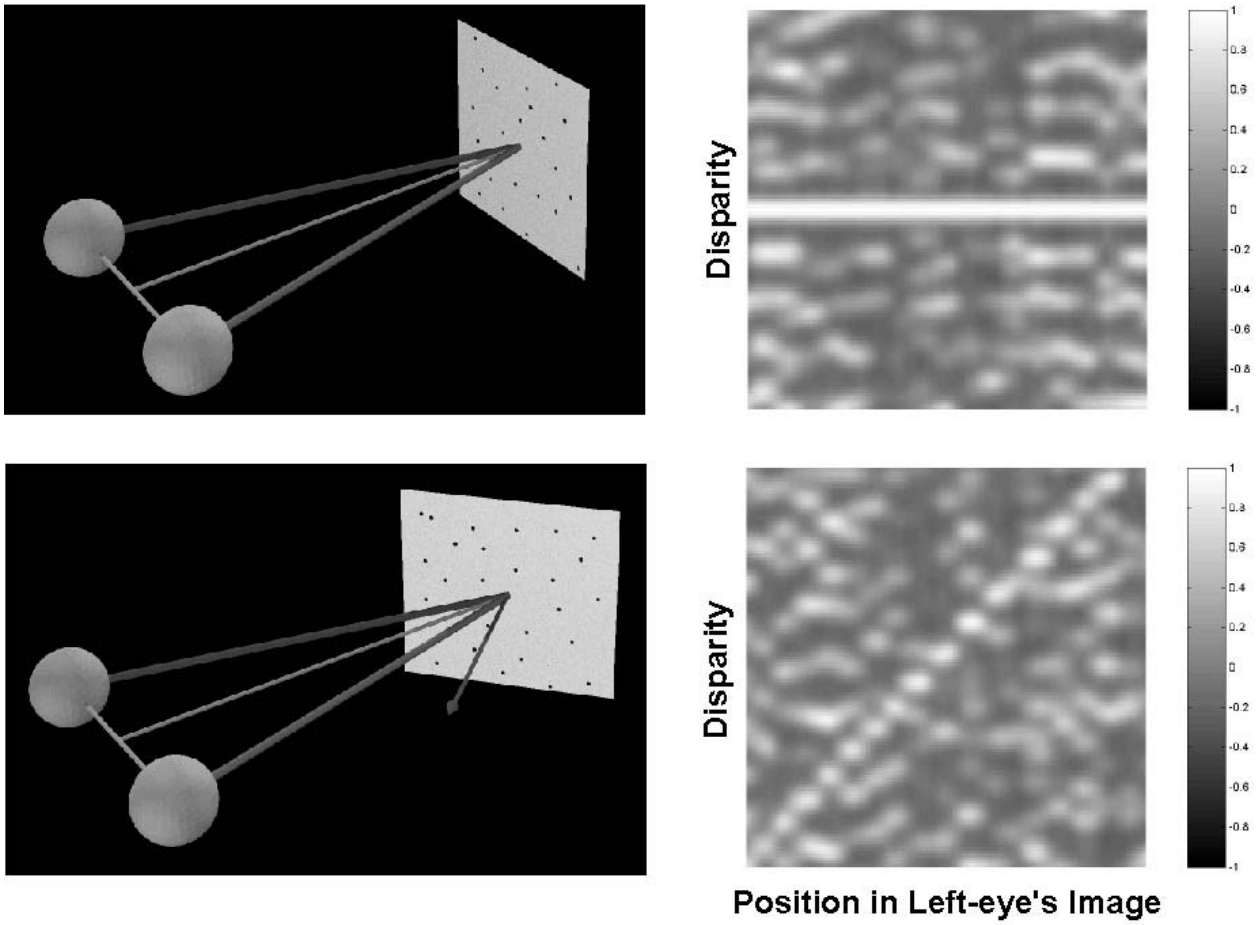

Figure 2. Model output as a function of stimulus slant. The two left panels show the viewing situations: a frontoparallel, textured plane in the upper panel and a slanted textured plane in the lower. The two right panels show the model's output for

those two viewing situations. The abscissae are the position of the correlation window in the left-eye's image. The ordinates are the position of the window in the right-eye's image; this corresponds to the horizontal disparity. The gray-scale values indicate the correlation at each position and disparity (color bars on the right).

The two left panels of Figure 2 are schematics of planes: a frontoparallel plane (disparity gradient = ~0) at the top, and a slanted plane (disparity gradient > 0) at the bottom. The right panels show the model's outputs when presented these stimuli. With the frontoparallel stimulus, there is a ridge of high inter-ocular correlation at a disparity of 0. Thus, the correspondence problem is solved and the disparities associated with this stimulus are estimated accurately. With the slanted stimulus, the correlations associated with the correct disparities are lower. The model's output is now noisy, meaning that disparity estimation in this case is uncertain. As the stimulus is slanted more, thereby increasing the disparity gradient, the output becomes yet noisier. At a gradient of ~1, the model fails to find a solution.

We examined the influence of the disparity gradient by examining the behavior of the correlation algorithm for different disparity amplitudes and found that the disparity gradient was the key determinant of the ability to estimate disparity accurately. Figure 3 illustrates how accurately the correlation algorithm was able to estimate the disparities associated with a plane as a function of disparity gradient. Estimation was inaccurate for gradients whose magnitudes were greater than 0.4.

We also examined the effect of the direction of the disparity gradient (the tilt) and found no obvious differences in the gradient magnitude at which estimation broke down. This is consistent with the psychophysical observation that the disparity-gradient limit is constant across directions (Burt & Julesz, 1980).

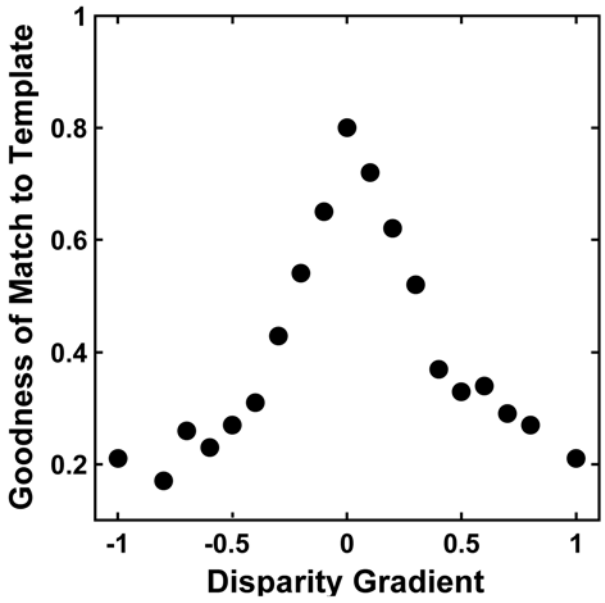

Figure 3. Reliability of disparity estimation as a function of disparity gradient. We ran the model (with untransformed left- and right-eye images) where the inputs were slanted planes like those in Figure 2. We constructed a template for each stimulus with the expected ridge of high disparity (right panels of Figures 1 & 2). We then measured the goodness of fit between the model's actual output and the expected output. The figure plots the goodness of fit as a function of disparity gradient.

One could construct a correlation algorithm that looked for slanted surface patches (disparity gradient ≠ 0) by transforming the monocular images according to the expected slant and tilt (expanding for tilt 0, shearing for tilt 90) in each image region before cross-correlating (Panton, 1978). We constructed such an algorithm and confirmed that it estimates disparity most accurately for the disparity gradient to which it is tuned. That is to say, the peak in Figure 3 shifted to the disparity gradient of the stimulus that yielded a disparity gradient of 0 after the monocular images were transformed. In summary, estimating disparity by correlating untransformed left- and right-eye images yields accurate estimates when the disparity gradient is low and successfully poorer estimates as the magnitude of the gradient increases. We speculate that the disparity-gradient limit is a consequence of this property of inter-ocular correlation.

V. EXPERIMENTAL TEST FOR THE SIGNIFICANCE OF THE DISPARITY GRADIENT

We conducted a psychophysical experiment to see if human stereo correspondence is similarly limited by the magnitude of the disparity gradient. The stimuli were presented on two high-resolution displays, one for each eye, in a custom stereoscope (Backus et al. 1999). The stimuli were random-dot stereograms with horizontal disparities specifying sawtooth corrugations in depth. Dot positioning was correct to within ~20 arcsec at a viewing distance of 39 cm. The high precision was achieved by spatial calibration (Backus et al., 1999) and anti-aliasing. The observer's eyes were placed in known positions with respect to the apparatus using a sighting technique (Hillis & Banks, 2001) and head position was stabilized with a bite bar. A central fixation dot helped maintain stable fixation.

The left side of Figure 4 is a schematic of the stimulus and the right side contains some example stereograms. The observers' task was to identify the spatial phase (0 or 180 deg) of the sawtooth corrugations. Waveform amplitude was varied from 10-160 minarc (peak to trough), and spatial frequency was varied from 0.15-0.6 cpd. At each combination of amplitude and spatial frequency, we varied the proportion of signal dots (specifying the sawtooth corrugation) vs noise dots (random in depth) in order to measure coherence thresholds (the number of signal dots divided by the total number of dots; total dot number was constant). An adaptive staircase controlled the proportion of signal dots. The generated data were used to find the best-fitting cumulative Gaussian via maximum likelihood (Wichmann & Hill, 2001). Threshold was the 75% point on those fitted Gaussians.

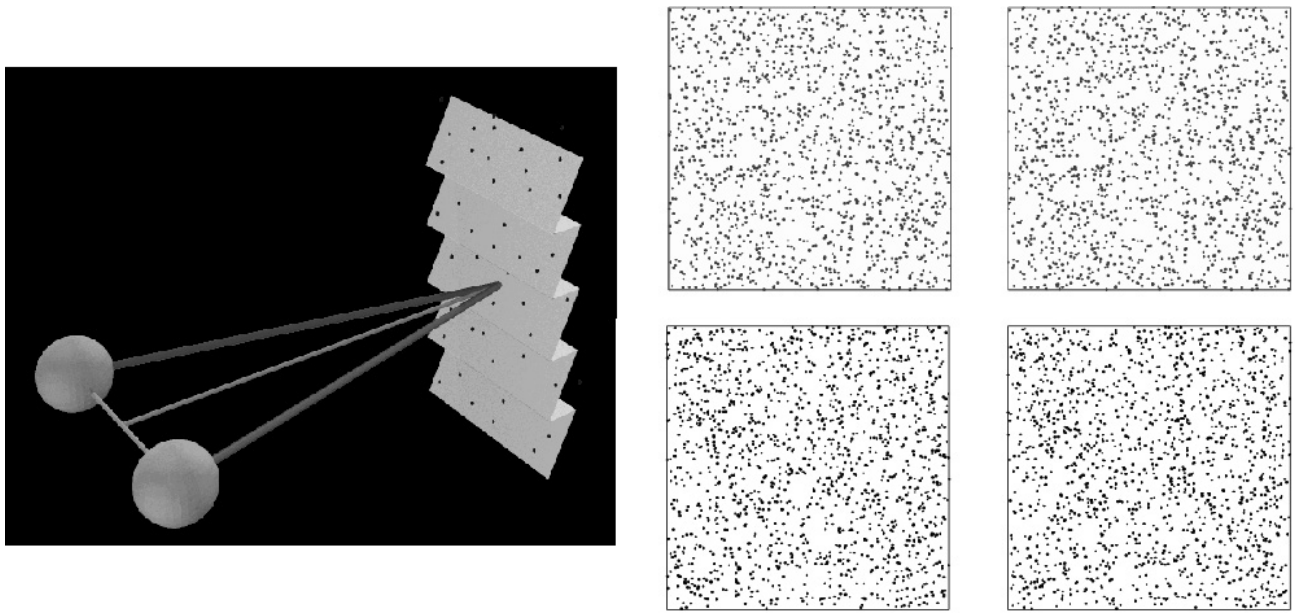

Figure 4. Left: Schematic of the sawtooth corrugation stimulus. The waveforms were defined by randomly positioned dots. The spatial phase of the corrugation was either 0 or 180 deg. Spatial frequency and disparity amplitude were independent variables in the experiment. The relative proportion of signal and noise (random depth) dots was the dependent variable. Right: Stereograms of the sawtooth corrugation waveform. The upper panel has no noise dots. The lower contains ~30% noise dots.

Ziegler et al. (2000) did a similar experiment. They measured d_{max}—the greatest peak-to-trough disparity for which the waveform could be seen—for sine, square, and trapezoidal waveforms. Their results are consistent with the idea that the disparity gradient is a critical limiting factor in detecting disparity-defined waveforms. But their experiment was not designed to test this hypothesis directly, so other interpretations are possible.

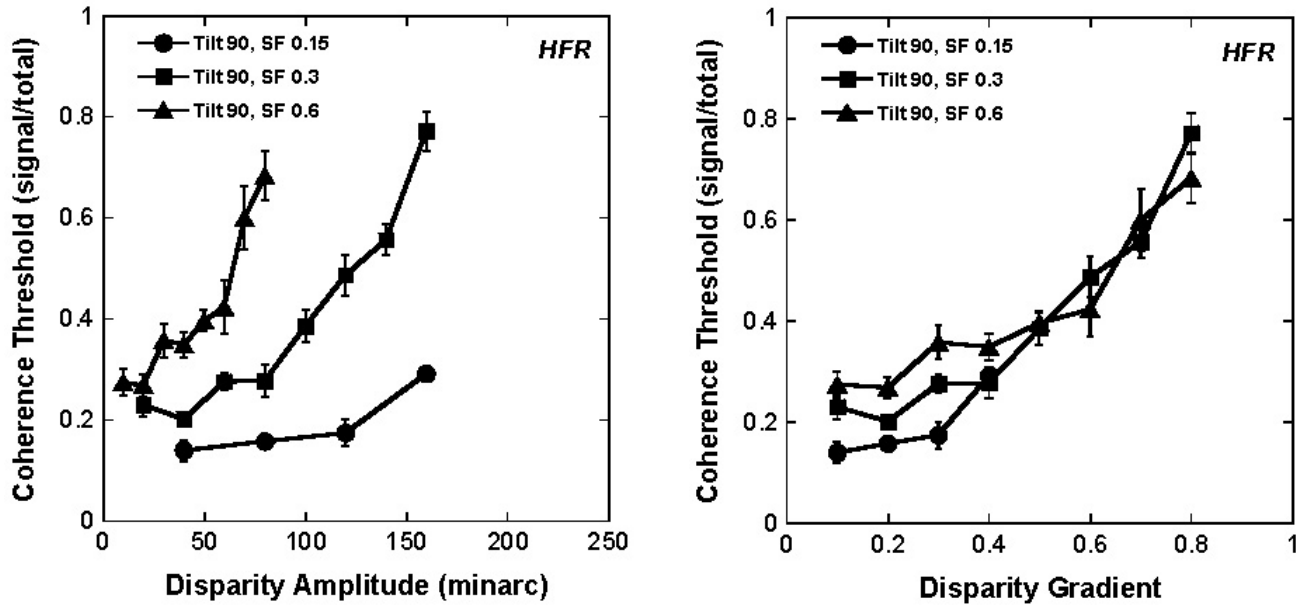

Figure 5. Experimental results from one observer. Left: Coherence threshold (the proportion of total dots that are signal dots at threshold) is plotted as a function of the disparity amplitude of the sawtooth waveform. Tilt was 90 deg. Spatial frequency was 0.15-0.6 cpd. Error bars represent +/- 1 standard error. Right: The same data plotted as a function of the disparity gradient. Because the waveforms were sawtooths, the disparity gradient was the amplitude divided by the spatial period.

Our results for one of the five observers are plotted in Figure 5. The left panel plots the data as a function of disparity amplitude and the right panel plots the same data as a function of the disparity gradient. Clearly, disparity gradient was a stronger determinant of coherence threshold than disparity amplitude was. When the disparity gradient reached a value of 0.4 or higher, coherence threshold rose steeply. That is to say, as the disparity gradient became larger through a combination of increasing spatial frequency and increasing amplitude, observers found it more difficult to discriminate the spatial phase of the waveform in the presence of noise. We observed the same results at tilt 0 (vertical corrugations) and tilt 90 (horizontal corrugations), and we observed the same results in the other four observers.

As we pointed out earlier, the behavior exemplified in Figure 5 is a consequence of using inter-ocular correlation of the untransformed left- and right-eye images to estimate disparity. We argue, therefore, that human observers use a method much like inter-ocular correlation to solve the stereo correspondence problem. We argue further that the disparity-gradient limit (Burt & Julesz, 1980), including the fact that the critical value does not depend on stimulus tilt, is a consequence of using inter-ocular correlation.

VI. CONCLUSIONS

A key feature of stereo matching by inter-ocular correlation is that the correlation is highest when the two eyes' images, once shifted horizontally into registration, are similar. Because of this, the highest correlations are observed when the disparity gradient is ~0, which can only occur in frontal gaze when the stimulus is frontoparallel (it is tangent to the Vieth-Müller Circle for all gaze eccentricities). We speculate that the visual system solves the binocular-matching problem with a procedure like the algorithm described here and, as a consequence, disparity estimates are those associated with piecewise frontal surface patches. Our modeling and psychophysical results support this idea.

In a study of disparity-selective cells in V1, Nienborg et al. (2004) came to the same conclusion. If V1 neurons are in fact not selective for slant and tilt, as Nienborg et al. propose, how are the slant- and tilt-selective neurons in extra-striate cortex created (Shikata et al., 1996; Nguyenkim & DeAngelis, 2003)? This could be done by combining the outputs of V1 neurons selective for piecewise frontal patches at different depths. With the right combination, a higher-order neuron selective for a particular magnitude and direction of disparity gradient could be constructed. Of course, such neurons could not have higher stereoresolution than observed among V1 neurons; the disparity-estimation process in V1 would be a resolution bottleneck. We believe our psychophysical results manifest this: Stereoresolution is relatively poor because binocular matching requires correlating the two eyes' images, and this in turn requires the use of mechanisms large enough to "see" enough intensity variation to compute a meaningful correlation.

VII. REFERENCES

Anzai A., Ohzawa I., & Freeman R.D. (1999). Neural mechanisms for processing binocular information I. Simple cells. *Journal of Neurophysiology* **82**, 891-908.

Backus, B.T., Banks, M.S., van Ee, R., & Crowell, J.A. (1999). Horizontal and vertical disparity, eye position, and stereoscopic slant perception. *Vision Research*, **39**, 1143-1170.

Banks, M.S., Gepshtein, S., & Landy, M.S. (2004). Why is spatial stereoresolution so low? *Journal of Neuroscience* **24**, 2077-2089.

Barnard, S.T. & Fischler, M.A. (1987). *Stereo vision* in *Encyclopedia of Artificial Intelligence*, New York: Wiley, pp. 1083-1090.

Braddick, O.J. (1979). Binocular single vision and perceptual processing. *Proceedings of the Royal Society of London B* **204**, 503-512.

Burt P. & Julesz, B. (1980). A disparity gradient limit for binocular fusion. *Science* **208**, 615-617.

Cormack, L.K., Stevenson, S.B., & Schor, C.M. (1991). Interocular correlation, luminance contrast and cyclopean processing. *Vision Research* **31**, 2195-2207.

Cox, I., Hingorani, S., & Roa, S. (1996). A maximum likelihood stereo algorithm. *Computer Vision and Image Understanding*, **63**, 542-567.

Cumming, B.G. & Parker, A.J. (1997). Responses of primary visual cortical neurons to binocular disparity without the perception of depth. *Nature* **389**, 280-283.

Ferster, D. (1981). A comparison of binocular depth mechanisms in areas 17 and 18 of the cat visual cortex. *Journal of Physiology* **311**, 623-655.

Fleet, D.J., Wagner, H., & Heeger, D.J. (1996). Neural encoding of binocular disparity: energy models, position shifts and phase shifts. *Vision Research* **36**, 1839-1857.

Grimson, W. (1981). *From images to surfaces: A computational study of the early human visual system*. Cambridge: MIT Press.

Hillis, J.M. & Banks, M.S. (2001). Are corresponding points fixed? *Vision Research* **41**, 2457-2473.

Jenkin, M.R.M. & Jepson, A.D. (1988). The measurement of binocular disparity. In *Computational processes in human vision: an interdisciplinary perspective*. Pylyshyn AW, Ed., Norwood, NJ: Ablex.

Julesz, B. (1971) *Foundations of Cyclopean Perception*. Chicago: University of Chicago.

Kanade T. & Okutomi M. (1994) A stereo matching algorithm with an adaptive window: theory and experiment. *IEEE Transactions for Pattern Analysis and Machine Intelligence* **16**, 920-932.

Marr, D. & Poggio, T. (1976). Cooperative computation of stereo disparity, *Science*, **194**, 283-287.

Marr, D. & Poggio, T. (1979). A computational theory of human stereo vision. *Proceedings of the Royal Society London B* **204**, 301-328.

Mayhew, J.E.W. & Frisby, J.P. (1980). The computation of binocular edges. *Perception* **9**, 69-86

Nelson, J.I. (1975). Globality and stereoscopic fusion in binocular vision. *Journal of Theoretical Biol.* **49**, 1-88.

Nguyenkim, J.D. & DeAngelis, G.C. (2003). Disparity-based coding of three-dimensional surface orientation by macaque middle temporal neurons. *Journal of Neuroscience* **23**, 7117-7128.

Nienborg, H., Bridge, H., Parker, A.J. & Cumming, B.G. (2004). Receptive field size in V1 neurons limits acuity for perceiving disparity modulation. *Journal of Neuroscience* **24**, 2065-2076.

Ogle, K.N. (1950). *Researches in Binocular Vision*. Saunders, Philadelphia.

Ohzawa I., DeAngelis, G.C., & Freeman, R.D. (1990). Stereoscopic depth discrimination in the visual cortex: neurons ideally suited as disparity detectors. *Science* **249,** 1037-1041.

Panton, D.J. (1978). A flexible approach to digital stereo mapping. *Photogram Engin Rem Sen* **44**, 1499-1512.

Pollard, S.B., Mayhew, J.E., & Frisby, J.P. (1985). PMF: a stereo correspondence algorithm using a disparity gradient limit. *Perception*, **14**, 449-470.

Prazdny, K. (1985). Detection of binocular disparities. *Biological Cybernetics* **52**, 93-99.

Prince, S.J., Pointon, A.D., Cumming, B.G., & Parker, A.J. (2002). Quantitative analysis of the responses of V1 neurons to horizontal disparity in random-dot stereograms. *Journal of Neuroscience*, **87**, 191-208.

Qian, N. & Zhu, Y.D. (1997). Physiological computation of binocular disparity. *Vision Research* **37**, 1811-1827.

Shikata, E., Tanaka, Y., Nakamura, H., Taira, M., & Sakata, H. (1996). Selectivity of the parietal visual neurons in 3D orientation of surface and stereoscopic stimuli. *Neuroreport* **7**, 2389-2394.

Trivedi, H.P. & Lloyd, S.A. (1985). The role of disparity gradient in stereo vision. *Perception*, **14**, 685-690.

Tyler, C.W. (1973). Stereoscopic vision: cortical limitations and a disparity scaling effect. *Science,* **181**, 276-278.

Tyler, C.W. & Julesz, B. (1978) Binocular cross-correlation in time and space. *Vision Research* **18**, 101-105.

Weinshall, D. & Malik, J. (1995). Review of computational models in stereopsis. In: *Early vision and beyond* (Papathomas TV, Chubb C, Gorea A, Kowler, E, eds), Cambridge: MIT Press.

Wichmann, F.A. & Hill, N.J. (2001). The psychometric function: I. Fitting, sampling, and goodness-of-fit. *Perception & Psychophysics* **63**, 1293-1313.

Ziegler, L.R., Hess, R.F., & Kingdom, F.A. (2000). Global factors that determine the maximum disparity for seeing cyclopean surface shape. *Vision Research*, **40**, 493-502.